

Two-body density matrix of a normal Fermi fluid

M. L. Ristig

Departamento de Física Moderna, Universidad de Granada, E-18071 Granada, Spain

J. W. Clark

McDonnell Center for the Space Sciences and Department of Physics, Washington University, St. Louis, Missouri 63130

(Received 21 August 1989)

The microscopic study of the two-body density matrix $\rho_2(\mathbf{r}_1, \mathbf{r}_2, \mathbf{r}'_1, \mathbf{r}'_2)$ initiated for uniform Bose fluids in an earlier paper is continued for the Fermi case. We present formal results on the structure of the generalized momentum distribution $n(\mathbf{p}, \mathbf{q}) = \sum_{\mathbf{k}} \langle \Psi | a_{\mathbf{k}+\mathbf{q}}^\dagger a_{\mathbf{p}-\mathbf{q}}^\dagger a_{\mathbf{p}} a_{\mathbf{k}} | \Psi \rangle$, and its Fourier inverse $\rho_2(\mathbf{r}_1, \mathbf{r}_2, \mathbf{r}'_1, \mathbf{r}'_2) \equiv \rho_2(\mathbf{r}_1, \mathbf{r}_2, \mathbf{r}'_1)$, based on a variational ground-state wave function of Jastrow-Slater form. The structural relations are inferred from the cluster expansions of these objects, from the asymptotic condition relating $\rho_2(\mathbf{r}_1, \mathbf{r}_2, \mathbf{r}'_1)$ to the particle density and the one-body density matrix $\rho_1(\mathbf{r}_1, \mathbf{r}'_1)$, and from formal diagrammatic connections with the Bose problem. The two-body density-matrix elements $\rho_2(\mathbf{r}_1, \mathbf{r}_2, \mathbf{r}'_1)$ are thereby expressed in closed form in terms of certain sums of irreducible cluster diagrams. Some of these diagram sums are familiar from the analogous theory of the one-body density matrix; all can be evaluated quantitatively by solving a set of Fermi-hypernetted-chain (FHNC) equations. Upon invoking the sequential relation between $\rho_2(\mathbf{r}_1, \mathbf{r}_2, \mathbf{r}'_1)$ and $\rho_1(\mathbf{r}_1, \mathbf{r}'_1)$, the corresponding result for the generalized momentum distribution $n(\mathbf{p}, \mathbf{q})$ effects a resolution into contributions from various scattering processes occurring in the many-body medium, specified by form factors that are susceptible to FHNC evaluation. This decomposition is comparable to that derived earlier for the Bose-fluid ground state but is complicated by contributions from exchange scattering and by a dynamically dressed Pauli kinematic correction. Silver has proposed a simple expression for the generalized momentum distribution $n(\mathbf{p}, \mathbf{q})$, a function which plays an essential role in his theory of final-state effects in deep-inelastic neutron scattering from the helium liquids. Based on the present microscopic treatment, the quality of Silver's estimate is assessed for the case of normal liquid ^3He , by evaluating the necessary distribution functions and form factors within the FHNC/0 approximation.

I. INTRODUCTION

Valuable information on the dynamic structure of quantum many-body systems like liquid helium may be derived from deep-inelastic scattering of neutrons and other weakly interacting probe particles. The experimental data from such scattering processes are conventionally analyzed in the impulse approximation.¹ The underlying assumption is that the probing neutron transfers momentum $\hbar\mathbf{k}$ and energy $\hbar\omega$ to a single atom of the helium target, the remaining atoms acting merely as spectators. As shown in Fig. 1, the struck atom is ejected with momentum $\hbar\mathbf{p}$. However, in helium the constituents are strongly correlated even at high momentum transfer. Although it remains legitimate to describe the process in terms of a collision of the probe with a single atom, the struck particle cannot be considered to recoil with the propagator of a free particle. Rather, it suffers "final-state interactions," which entail scatterings with particles of the medium, leading from momentum state $\hbar\mathbf{p}$ to another final state of momentum $\hbar(\mathbf{p}-\mathbf{q})$. The novel theory proposed and applied by Silver²⁻⁵ suggests that these final-state interactions are dominated by the exchange of a virtual phonon, i.e., a density fluctuation of the structured helium target. Figure 2 sketches the corresponding scattering process, wherein the phonon acts to conserve

momentum. Strong evidence for this mechanism is provided by the spectacular agreement between theoretical and experimental results for the neutron-scattering Compton profile function $J(Y)$ in liquid ^4He at the highest momentum transfers, when final-state interactions are incorporated in the theoretical prediction using Silver's theory.⁶ On the other hand, the numerical analysis of Refs. 2-6 employs rather crude approximations for the form factors that govern the indicated scattering process. A quantitative test of the current understanding of the dynamics of deep-inelastic scattering requires accurate calculation of these form factors by microscopic many-body methods.

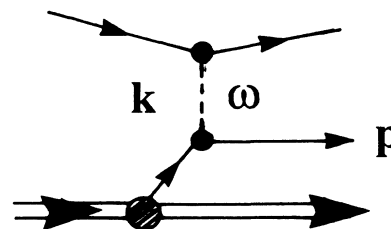


FIG. 1. Deep-inelastic scattering of neutrons from normal liquid ^3He , as described within the impulse approximation.

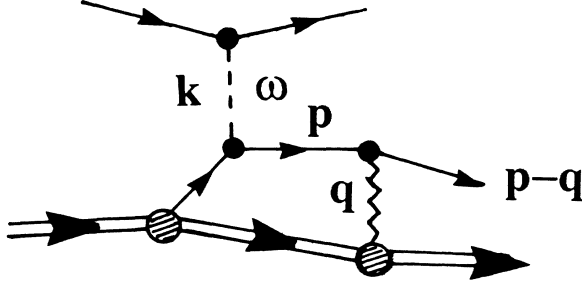


FIG. 2. Deep-inelastic scattering of neutrons from normal liquid ${}^3\text{He}$, involving final-state interactions mediated by a density fluctuation of the target ${}^3\text{He}$ system (a phonon of wave vector q).

This paper is the second of two that are devoted to formal and numerical evaluation of the form factors describing the final-state mechanism of Fig. 2. The form factors associated with the processes shown in Figs. 1 and 2 may be extracted from the single-particle momentum distribution $n(p)$ and from the generalized momentum distribution function $n(\mathbf{p}, \mathbf{q})$ characterizing the target system, which are in turn determined by the one- and two-body density matrices $\rho_1(\mathbf{r}_1, \mathbf{r}'_1)$ and $\rho_2(\mathbf{r}_1, \mathbf{r}_2, \mathbf{r}'_1, \mathbf{r}'_2)$ of the correlated ground state of the system. A detailed study of these quantities for the case of a uniform, isotropic fluid of spinless bosons has been presented in the first paper, Ref. 7. Here, we shall report the results of an analogous study for Fermi fluids. The formalism is applied in a numerical evaluation of the form factors of the final-state scattering process depicted in Fig. 2, with liquid ${}^3\text{He}$ as target. The formalism (with some modifications for finite target size and state-dependent ground-state correlations) may also be applied to the problem of final-state effects in quasielastic electron-nucleus scattering and other probe-target scattering scenarios.⁸⁻¹³ However, other mechanisms may well be more important in the nuclear context than the phonon-induced process of Fig. 2.

Let us recall the definitions of the momentum $\hbar\mathbf{p}$ distribution functions $n(p)$ and $n(\mathbf{p}, \mathbf{q})$, which will be the primary objects of our analysis. The former is the occupation probability

$$n(p) = \langle \Psi | a_{\hat{p}}^\dagger a_{\hat{p}} | \Psi \rangle \quad (1)$$

for a single-particle orbital \hat{p} of momentum $\hbar\mathbf{p}$ and spin projection σ . The correlated ground-state wave function Ψ (which we assume is normalized to unity) must be completely antisymmetric in the case of a Fermi system. We are interested in the unpolarized normal ground state of liquid ${}^3\text{He}$, so the spin degeneracy is taken as $\nu=2$ with $\sigma=\uparrow$ or \downarrow . The generalized momentum distribution $n(\mathbf{p}, \mathbf{q})$ is defined by

$$n(\mathbf{p}, \mathbf{q}) = \sum_{\hat{\mathbf{k}}} \langle \Psi | a_{\hat{\mathbf{k}}+\mathbf{q}}^\dagger a_{\hat{\mathbf{p}}-\mathbf{q}}^\dagger a_{\hat{\mathbf{p}}} a_{\hat{\mathbf{k}}} | \Psi \rangle, \quad (2)$$

where $\hat{\mathbf{p}}-\mathbf{q}=(\mathbf{p}-\mathbf{q}, \sigma)$ and $\hat{\mathbf{k}}+\mathbf{q}=(\mathbf{k}+\mathbf{q}, \sigma')$, and we have averaged over all momenta $\hbar\mathbf{k}$ and spin projections σ' of orbital $\hat{\mathbf{k}}$. The quantity (2) is directly involved in the final-state mechanism represented by Fig. 2, as may

be seen by introducing the density fluctuation operator $\rho_{\mathbf{q}} = \sum_{\hat{\mathbf{k}}} a_{\hat{\mathbf{k}}+\mathbf{q}}^\dagger a_{\hat{\mathbf{k}}}$ (with $\mathbf{q} \neq 0$) and writing Eq. (2) in the form

$$n(\mathbf{p}, \mathbf{q}) = \langle \Psi | \rho_{\mathbf{q}} a_{\hat{\mathbf{p}}-\mathbf{q}}^\dagger a_{\hat{\mathbf{p}}} | \Psi \rangle - n(p). \quad (3)$$

As in the Bose case considered in Ref. 7, the expectation value (3) may be interpreted as a transition matrix element for scattering a particle out of orbital \hat{p} to another orbital $\hat{p}-\mathbf{q}$ (without a spin flip), the process being mediated by a (spin-independent) density fluctuation (see Fig. 3). Evidently, this transition just corresponds to the final-state scattering process occurring at the rightmost single-atom vertex in Fig. 2. The Fermi problem differs from the Bose case studied earlier in the obvious respect that processes involving creation of a particle out of (absorption of a particle into) a zero-momentum condensate no longer appear, since, in contrast to the situation for a Bose fluid, a Fermi fluid does not display off-diagonal long-range order of the one-body density matrix. We may further point out that if spin-dependent correlations are important, one should consider more general quantities than (2), for example spin-dependent versions of this quantity in which the sum over $\hat{\mathbf{k}}=\mathbf{k}, \sigma$ is replaced by a sum over the momentum \mathbf{k} alone, or in which no sum is performed.

Ignoring kinematic as well as dynamic correlations between and among the N fermionic constituents of the fluid, the generalized momentum distribution (2) takes the simple form

$$n_0(\mathbf{p}, \mathbf{q}) = \delta_{\mathbf{q}0} (N-1) n(p), \quad (4)$$

which recovers the impulse approximation. This result holds equally well for Bose fluids.⁷ However, if we specify merely that the particles are noninteracting, we must take account of the fact that the Pauli exclusion principle generates kinematic particle-particle correlations, leading instead to a generalized momentum distribution function

$$n_F(\mathbf{p}, \mathbf{q}) = \delta_{\mathbf{q}0} (N-1) \Theta(k_F - p) - (1 - \delta_{\mathbf{q}0}) \Theta(k_F - p) \Theta(k_F - |\mathbf{p}-\mathbf{q}|), \quad (5)$$

where k_F is the Fermi wave number. (No such kinematic effects arise from the statistics of the Bose problem). Correspondingly, if we ignore dynamical but not kinematic correlations, the Fermi occupation probability (1) is given simply by the Hartree-Fock distribution $n_F(p) = \Theta(k_F - p)$.

In the presence of interactions, $n_F(p)$ and both terms of

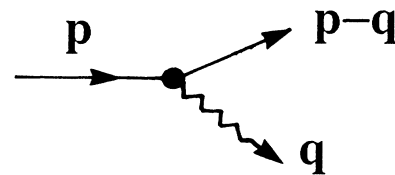


FIG. 3. Graphical representation of the transition matrix element $\langle \Psi | \rho_{\mathbf{q}} a_{\hat{\mathbf{p}}-\mathbf{q}}^\dagger a_{\hat{\mathbf{p}}} | \Psi \rangle$ of Eq. (3). A fermion is scattered from orbital \hat{p} into another orbital $\hat{p}-\mathbf{q}$ by a phonon.

$n_F(\mathbf{p}, \mathbf{q})$ will be dressed by dynamic correlations. A complete theory of the distribution function (2) must, of course, also incorporate the phonon-mediated scattering process shown in Fig. 3 [cf. Eq. (3)], which arises from the correlation structure of the medium. The contributions from the pertinent physical effects, both kinematic and dynamic, will be given explicit expression in the following sections, in terms of various dressed quantities and form factors which are amenable to microscopic evaluation. The results furnish the microscopic information about the ground state that is required for a determination of the final-state correction to the impulse approximation corresponding to Fig. 2.

The analysis begins with an appropriate cluster development of the generalized momentum distribution $n(\mathbf{p}, \mathbf{q})$. The cluster analysis draws on the same techniques and notations as were introduced in our earlier study¹⁴ of the momentum distribution (1). The results are transformed to \mathbf{r} space to obtain the corresponding cluster contributions to the two-body density-matrix elements $\rho_2(\mathbf{r}_1, \mathbf{r}'_1, \mathbf{r}_2)$. Fermi-hypernetted-chain (FHNC) resummations may be performed in the standard manner^{15,16} to elucidate the structure of $n(\mathbf{p}, \mathbf{q})$ and $\rho_2(\mathbf{r}_1, \mathbf{r}'_1, \mathbf{r}_2)$. In particular, we achieve a systematic decomposition of the generalized momentum distribution into contributions from the dynamical and statistical effects already indicated. Within this decomposition, form factors for scattering processes occurring in the medium are identified and constructed explicitly in terms of a set of (more or less familiar) irreducible two- and three-point functions, which also serve to generate $\rho_1(\mathbf{r}_1, \mathbf{r}'_1)$ and $\rho_2(\mathbf{r}_1, \mathbf{r}_2, \mathbf{r}'_1)$. The formal analysis paves the way for an accurate evaluation of the required form factors as functions of the relevant momenta. Much that was learned in the companion paper on Bose fluids⁷ can be carried over without change to the present context of normal Fermi fluids (or with minor changes of an obvious nature).

As a first numerical application of the formalism, certain form factors have been calculated in a Fermi-hypernetted-chain treatment in which elementary diagrams are neglected. The results permit a test of the accuracy of the simple approximation to $n(\mathbf{p}, \mathbf{q})$ that has been implemented in Silver's evaluation of final-state effects in deep-inelastic scattering. In our calculation, the ground state of liquid ³He is described by a Jastrow-Slater variational wave function containing two-body correlations of the simple Schiff-Verlet type.^{17,18}

Section II sketches the derivation of a cluster expansion for the generalized momentum distribution based on standard procedures.^{19,20} The FHNC analysis of the associated two-body density-matrix elements is presented in Sec. III. In Sec. IV we extract the form factors corresponding to the phonon-induced scattering process and the particle-particle Pauli exchange corrections. The final section reports numerical results on form factors in liquid ³He.

II. CLUSTER EXPANSIONS

The momentum distribution (1) has been the subject of intensive theoretical study and has been calculated for a

variety of helium, nuclear, and electronic systems by means of advanced many-body methods. A recent review of efforts toward quantitative microscopic prediction of $n(p)$ may be found in Ref. 21. In the present contribution we shall initiate the microscopic treatment of the more complex quantity (2), for the case of Fermi statistics, exploiting the techniques developed in Refs. 7 and 14 for $n(p)$ and for the Bose version of $n(\mathbf{p}, \mathbf{q})$, and making use of the same (or similar) notation and diagrammatic representations. As in Ref. 14, we approximate the ground state of N strongly interacting fermions by a variational wave function of the Jastrow-Slater type and evaluate the associated generalized momentum distribution (2) in terms of cluster approximants. Specifically, the model ground-state wave function is

$$\Psi = \mathcal{N}^{-1} \prod_{i < j}^N f(r_{ij}) \Phi, \quad (6)$$

where Φ is a Slater determinant of plane-wave orbitals, describing the ground state of the corresponding free Fermi gas of particle density $\rho = \nu k_F^3 / 6\pi^2$ and single-particle level degeneracy ν , and $f(r_{ij})$ is a Jastrow pair correlation function depending only on the scalar separation of particles i, j . The constant \mathcal{N} , taken as the norm of $\prod f \Phi$, is introduced to normalize Ψ to unity.

The developments of this and subsequent sections may be generalized in a straightforward manner to deal with a more elaborate ground-state trial function in which the Jastrow correlation factor in (6) is replaced by a Feenberg function²² involving irreducible spatial correlations between triples, quadruples, etc., of particles as well as pairs. The analysis would lead to essentially the same structural results for the generalized distribution function and associated density-matrix elements, with the qualification that the diagrammatic content of the various functions involved is much richer.

Cluster decomposition of (2) is facilitated by recasting this quantity in the form

$$n(\mathbf{p}, \mathbf{q}) = \delta_{q0} (N - 1) n(p) + (1 - \delta_{q0}) \langle \Psi | N(\hat{\mathbf{p}}, \mathbf{q}) | \Psi \rangle, \quad (7)$$

where

$$2N(\hat{\mathbf{p}}, \mathbf{q}) = \rho_q a_{\hat{\mathbf{p}}-\mathbf{q}}^\dagger a_{\hat{\mathbf{p}}} + a_{\hat{\mathbf{p}}-\mathbf{q}}^\dagger a_{\hat{\mathbf{p}}} \rho_q - a_{\hat{\mathbf{p}}}^\dagger a_{\hat{\mathbf{p}}} - a_{\hat{\mathbf{p}}-\mathbf{q}}^\dagger a_{\hat{\mathbf{p}}-\mathbf{q}}. \quad (8)$$

It is to be noted that the operator $N(\hat{\mathbf{p}}, \mathbf{q})$ is not self-adjoint; rather, $N^\dagger(\hat{\mathbf{p}}, \mathbf{q}) = N(\hat{\mathbf{p}} - \mathbf{q}, -\mathbf{q})$.

The first term in (7) is responsible for the independent-fermion (or impulse-approximation) expression (4). Hence the effects of two-body correlations, except as they influence $n(p)$, must be entirely due to the nonzero expectation value of the operator $N(\hat{\mathbf{p}}, \mathbf{q})$ of (8). Indeed, at constant total particle number we may express this operator as a sum of $N(N-1)/2$ two-body operators,

$$N(\hat{\mathbf{p}}, \mathbf{q}) = \sum_{i < j}^N N_{\hat{\mathbf{p}}\mathbf{q}}(i, j). \quad (9)$$

The operator referring to fermions i and j (acting in the direct sum of their Hilbert spaces, with $i \neq j$) is

$$N_{\hat{\mathbf{p}}\mathbf{q}}(ij) = e^{iq\cdot\mathbf{r}_i} o_{\hat{\mathbf{p}}-\mathbf{q},\hat{\mathbf{p}}}(j) + e^{iq\cdot\mathbf{r}_j} o_{\hat{\mathbf{p}}-\mathbf{q},\hat{\mathbf{p}}}(i), \quad (10)$$

the action of the one-body operator $o_{\hat{\mathbf{p}}-\mathbf{q},\hat{\mathbf{p}}}(i)$ on the plane-wave orbital $|\hat{\mathbf{k}}^{(i)}\rangle$ being defined by

$$o_{\hat{\mathbf{p}}-\mathbf{q},\hat{\mathbf{p}}}|\hat{\mathbf{k}}\rangle = \delta_{\hat{\mathbf{p}}\hat{\mathbf{k}}|\hat{\mathbf{p}}-\mathbf{q}}, \quad \langle\hat{\mathbf{k}}|o_{\hat{\mathbf{p}}-\mathbf{q},\hat{\mathbf{p}}} = \delta_{\hat{\mathbf{k}},\hat{\mathbf{p}}-\mathbf{q}}\langle\hat{\mathbf{p}}|. \quad (11)$$

We are now in a position to invoke the standard procedures for cluster expanding the expectation value of a sum of two-body operators, the most familiar example being the potential energy corresponding to a sum of pair potentials.²⁰ In the thermodynamic limit—meaning that the particle number N goes to infinity while the particle density ρ is kept constant—the generalized distribution function (2) and (7) is decomposed into an infinite series of cluster terms,

$$n(\mathbf{p}, \mathbf{q}) = n_F(\mathbf{p}, \mathbf{q}) + (1 - \delta_{q0})[n_{(2)}(\mathbf{p}, \mathbf{q}) + n_{(3)}(\mathbf{p}, \mathbf{q}) + \dots]. \quad (12)$$

The specific procedures applied in the present work have been described at length in Ref. 14, which the reader should consult for details. The cluster contributions $n_{(2)}(\mathbf{p}, \mathbf{q})$, $n_{(3)}(\mathbf{p}, \mathbf{q})$, ... appearing in (12) are most conveniently represented by generalized Ursell-Mayer diagrams.^{20,23} The basic diagram rules and some examples are given in the Appendix. Figure 4 displays the contributions to the two-body cluster term $n_{(2)}(\mathbf{p}, \mathbf{q})$. The three-body cluster term $n_{(3)}(\mathbf{p}, \mathbf{q})$ is represented by 138 such Ursell-Mayer diagrams (not shown because of the prohibitive space required). However, most of these diagrams are reducible, as becomes apparent when we examine the m -body cluster contribution in coordinate space, i.e., the quantity $\rho_{2(m)}(\mathbf{r}_1, \mathbf{r}_2, \mathbf{r}'_1)$ defined by

$$n_{(m)}(\mathbf{p}, \mathbf{q}) = \frac{1}{v} \frac{\rho}{N} \int \rho_{2(m)}(\mathbf{r}_1, \mathbf{r}_2, \mathbf{r}'_1) e^{-i\mathbf{p}\cdot(\mathbf{r}_1 - \mathbf{r}'_1)} \times e^{-iq\cdot(\mathbf{r}_1 - \mathbf{r}_2)} d\mathbf{r}_1 d\mathbf{r}_2 d\mathbf{r}'_1. \quad (13)$$

Transformation of individual cluster contributions to $n_{(m)}(\mathbf{p}, \mathbf{q})$ into their coordinate-space counterparts in $\rho_{2(m)}(\mathbf{r}_1, \mathbf{r}_2, \mathbf{r}'_1)$ may be easily accomplished graphically: Taking each diagram of $n_{(m)}(\mathbf{p}, \mathbf{q})$ in turn, one simply removes the arrows representing specific plane-wave orbitals and changes the (solid) field points that they originally intersected into (open) root points. Applying this graphical process to the sum of two-body cluster diagrams in Fig. 4, we obtain the \mathbf{r} -space counterpart $\rho_{2(2)}(\mathbf{r}_1, \mathbf{r}_2, \mathbf{r}'_1)$ shown in Fig. 5. The three-body cluster contribution

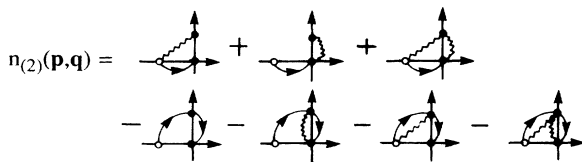


FIG. 4. Diagrammatic representation of the two-body cluster contributions to the generalized momentum distribution function $n(\mathbf{p}, \mathbf{q})$.

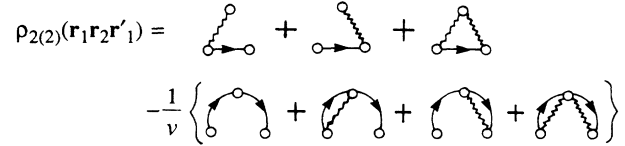


FIG. 5. Diagrammatic representation of the two-body cluster contributions to the Fourier inverse of the generalized momentum distribution function, i.e., to the two-body density-matrix elements $\rho_2(\mathbf{r}_1, \mathbf{r}_2, \mathbf{r}'_1)$.

$\rho_{2(3)}(\mathbf{r}_1, \mathbf{r}_2, \mathbf{r}'_1)$, derived same manner from $n_{(3)}(\mathbf{p}, \mathbf{q})$, is depicted in Fig. 6. The reducibility of a large share of the diagrams is evident in the presence of products of graphs.

In order to infer the characteristic structure of expansion (12), and of the corresponding expansion of the coordinate-space representation, we have examined selected classes of contributions in four-body cluster order. For the sake of economy, we do not display the complicated diagrams which enter at this order. At any rate, with the benefit of some technical experience, the selected diagrams—together with the results in two- and three-body orders—are sufficient to reveal the structure of the relevant cluster expansions out to infinite order. The results of this synthesis are presented in the next section.

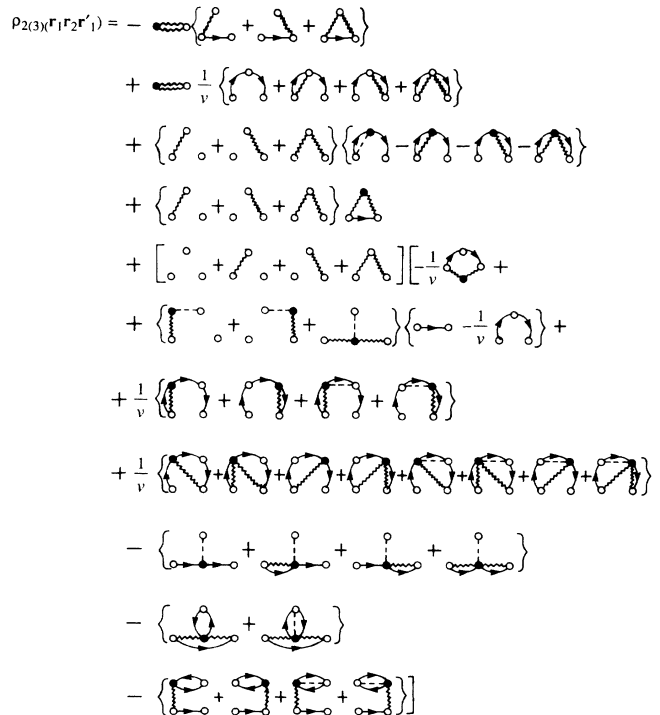


FIG. 6. Diagrammatic representation of the three-body cluster contributions to the two-body density-matrix elements $\rho_2(\mathbf{r}_1, \mathbf{r}_2, \mathbf{r}'_1)$.

III. FERMI-HYPERNETTED-CHAIN ANALYSIS > AM

The formal development now aims toward the resummation of cluster expansion (12) by hypernetted-chain techniques. It is most efficient to work in coordinate space, focusing on the two-body density matrix $\rho_2(\mathbf{r}_1, \sigma_1, \mathbf{r}_2, \sigma_2, \mathbf{r}'_1, \sigma'_1, \mathbf{r}'_2, \sigma'_2)$ corresponding to the chosen wave function of the Fermi fluid, or more specifically on the reduced version $\rho_2(\mathbf{r}_1, \mathbf{r}_2, \mathbf{r}'_1, \mathbf{r}'_2)$ in which all spin traces have been performed. Actually, in a study of the generalized momentum distribution function $n(\mathbf{p}, \mathbf{q})$ of (2) or (12) we only need the partially diagonal portion $\rho_2(\mathbf{r}_1, \mathbf{r}_2, \mathbf{r}'_1) = \rho_2(\mathbf{r}_1, \mathbf{r}_2, \mathbf{r}'_1, \mathbf{r}_2)$ of the latter quantity, since

$$n(\mathbf{p}, \mathbf{q}) = \frac{1}{v} \frac{\rho}{N} \int \rho_2(\mathbf{r}_1, \mathbf{r}_2, \mathbf{r}'_1) e^{-i\mathbf{p} \cdot (\mathbf{r}_1 - \mathbf{r}'_1)} \times e^{-i\mathbf{q} \cdot (\mathbf{r}_1 - \mathbf{r}_2)} d\mathbf{r}_1 d\mathbf{r}_2 d\mathbf{r}'_1. \quad (14)$$

Our characterization of the structure of $\rho_2(\mathbf{r}_1, \mathbf{r}_2, \mathbf{r}'_1)$ relies upon certain known properties of the cluster terms (13), together with (i) features of the asymptotic behavior of the elements $\rho_2(\mathbf{r}_1, \mathbf{r}_2, \mathbf{r}'_1)$ and (ii) relationships between these elements and their Bose counterparts (cf. Ref. 7). The more complicated quantity $\rho_2(\mathbf{r}_1, \sigma_1, \mathbf{r}_2, \sigma_2, \mathbf{r}'_1, \sigma'_1, \mathbf{r}'_2, \sigma'_2)$ may be dealt with in a similar manner.

The explicit diagrammatic analysis of the cluster ex-

pansion of $\rho_2(\mathbf{r}_1, \mathbf{r}_2, \mathbf{r}'_1)$ [involving Eqs. (12) and (13) in conjunction with Figs. 5 and 6, plus special four-body diagrams] suggests the general structural decomposition

$$\rho_2(\mathbf{r}_1, \mathbf{r}_2, \mathbf{r}'_1) = \rho_{2D}(\mathbf{r}_1, \mathbf{r}_2, \mathbf{r}'_1) [L(\mathbf{r}_1, \mathbf{r}'_1) + L(\mathbf{r}_1, \mathbf{r}_2, \mathbf{r}'_1)]. \quad (15)$$

The first factor collects the direct-direct portions of the full set of diagrams contributing to $\rho_2(\mathbf{r}_1, \mathbf{r}_2, \mathbf{r}'_1)$. By definition,²⁰ direct-direct diagrams do not have exchange lines attached to any of the root (or reference) points \mathbf{r}_1 , \mathbf{r}_2 , and \mathbf{r}'_1 . The complementary set of graphs contains only diagrams with exchange lines beginning and/or ending at two or three reference points. Of these graphs, the ones with exchange lines at two reference points combine to form the two-point exchange factor $L(\mathbf{r}_1, \mathbf{r}'_1)$, while the graphs with exchange lines at all three reference points compose the three-point function $L(\mathbf{r}_1, \mathbf{r}_2, \mathbf{r}'_1)$. Either of these exchange functions vanishes if any one of the coordinates in its argument recedes to an infinite distance from the others. In the Bose limit, obtained for level degeneracy $v \rightarrow \infty$ with $k_F \rightarrow 0+$ at constant density ρ , the function $L(\mathbf{r}_1, \mathbf{r}'_1)$ approaches unity and the three-point function $L(\mathbf{r}_1, \mathbf{r}_2, \mathbf{r}'_1)$ goes to zero. As expected, only the direct-direct contribution ρ_{2D} survives. Returning to finite v , this component of (15) may be compared, at a diagrammatic level, with the structural result that was derived for the Bose-fluid $\rho_2(\mathbf{r}_1, \mathbf{r}_2, \mathbf{r}'_1)$ in Ref. 7. We arrive thereby at the representation

$$\rho_{2D}(\mathbf{r}_1, \mathbf{r}_2, \mathbf{r}'_1) = \rho \rho_{1D}(\mathbf{r}_1, \mathbf{r}'_1) f(|\mathbf{r}_1 - \mathbf{r}_2|) f(|\mathbf{r}'_1 - \mathbf{r}_2|) \exp[-P(\mathbf{r}_1, \mathbf{r}_2) - P(\mathbf{r}'_1, \mathbf{r}_2) - P(\mathbf{r}_1, \mathbf{r}_2, \mathbf{r}'_1)]. \quad (16)$$

The generating functions $P(\mathbf{r}_1, \mathbf{r}_2) = P(|\mathbf{r}_1 - \mathbf{r}_2|) \equiv P(r)$ and $P(\mathbf{r}_1, \mathbf{r}_2, \mathbf{r}'_1)$ are irreducible quantities—sums of irreducible diagrams—just as in the Bose case. Figure 7 gives the leading cluster contributions to these functions. In fact, the diagrams shown do not differ from the leading diagrams that occur for the Bose fluid. However, as in the familiar example of the one-body density matrix $\rho_1(\mathbf{r}_1, \mathbf{r}'_1)$, additional, non-Bose diagrams will arise from the systematic introduction of exchange insertions at the field points of the Bose diagrams of higher orders.^{20,14}

The function $\rho_{1D}(\mathbf{r}_1, \mathbf{r}'_1)$ entering (16) is just the direct-direct component of the full Fermi one-body density matrix $\rho_1(\mathbf{r}_1, \mathbf{r}'_1)$. The structure of ρ_{1D} is well known from previous work.¹⁴⁻¹⁶ This quantity is generated by the irreducible phase-phase correlation function $Q(\mathbf{r}_1, \mathbf{r}'_1)$ (see Fig. 7, and Figs. 8 and 10 of Ref. 14), according to

$$\rho_{1D}(\mathbf{r}_1, \mathbf{r}'_1) = \rho n_0 \exp[-Q(\mathbf{r}_1, \mathbf{r}'_1)], \quad (17)$$

where $n_0 = \exp Q(\mathbf{r}_1, \mathbf{r}_1)$ is an overall strength factor.

The functions $Q(r)$, $P(r)$, and $P(\mathbf{r}_1, \mathbf{r}_2, \mathbf{r}'_1)$ (where, and throughout, $r \equiv |\mathbf{r}_1 - \mathbf{r}_2|$) may be resolved into nodal and elementary contributions,²⁰

$$\begin{aligned} -Q(r) &= N_{QQ}(r) + E_{QQ}(r), \\ -P(r) &= N_Q(r) + E_Q(r), \\ -P(\mathbf{r}_1, \mathbf{r}_2, \mathbf{r}'_1) &= N_Q(\mathbf{r}_1, \mathbf{r}_2, \mathbf{r}'_1) + E_Q(\mathbf{r}_1, \mathbf{r}_2, \mathbf{r}'_1), \end{aligned} \quad (18)$$

in analogy to the nodal-elementary separation of these quantities in the Bose case.^{15,16} Figure 7 shows the leading diagrams of nodal (N) type. Elementary (E) diagrams, contributing to $E_{QQ}(r)$, $E_Q(r)$, and $E_Q(\mathbf{r}_1, \mathbf{r}_2, \mathbf{r}'_1)$, will first appear in the next cluster order (not explicitly shown).

Concentrating next on the exchange factors $L(\mathbf{r}_1, \mathbf{r}'_1)$ and $L(\mathbf{r}_1, \mathbf{r}_2, \mathbf{r}'_1)$, we consider the limit $\mathbf{r}_2 \rightarrow \infty$ and exploit

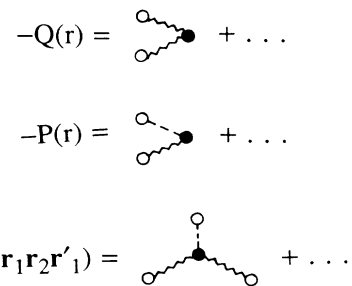


FIG. 7. Diagrammatic representation of the cluster expansions of the irreducible direct functions $Q(r)$, $P(r)$, and $P(\mathbf{r}_1, \mathbf{r}_2, \mathbf{r}'_1)$ (leading cluster contributions shown explicitly).

the asymptotic condition

$$\lim_{r_2 \rightarrow \infty} \rho_2(\mathbf{r}_1, \mathbf{r}_2, \mathbf{r}'_1) = \rho \rho_1(\mathbf{r}_1, \mathbf{r}'_1). \quad (19)$$

This relation should hold under very general assumptions on the interactions within the fluid, which are supposed to become vanishingly small at asymptotically large interparticle separations. If particle 2 is far from particle 1, the correlations between them should be negligible, and hence Eq. (19) should apply. The structure

$$\rho_1(\mathbf{r}_1, \mathbf{r}'_1) = \rho_{1D}(\mathbf{r}_1, \mathbf{r}'_1) [L_1(\mathbf{r}_1, \mathbf{r}'_1) + L_2(\mathbf{r}_1, \mathbf{r}'_1)] \quad (20)$$

of the one-body density matrix appearing on the right-hand side of (19) is well known,¹⁴⁻¹⁶ in terms of the direct-direct component ρ_{1D} of (17) and the exchange functions L_1 and L_2 . The exchange functions L_1 and L_2 are in turn known, both formally and numerically, within the FHNC scheme.^{15,16} The diagrams contributing to these functions through three-body cluster order are given in Fig. 8. [The functions L_1 and L_2 were originally denoted N_1 and N_2 (Ref. 14)].

Going to the asymptotic regime $r_2 \rightarrow \infty$ in expressions (15) and (16), and comparing with (19) and (20), we make the identification

$$L(\mathbf{r}_1, \mathbf{r}'_1) = L_1(\mathbf{r}_1, \mathbf{r}'_1) + L_2(\mathbf{r}_1, \mathbf{r}'_1). \quad (21)$$

$$\begin{aligned} L(\mathbf{r}_1, \mathbf{r}_2, \mathbf{r}'_1) = & +v^{-1}l(r)l(r') - l(r)[P_{cc}(r') - P_{dcc}(\mathbf{r}_1, \mathbf{r}_2, \mathbf{r}'_1)] - l(r')[P_{cc}(r) + P_{dcc}(\mathbf{r}_1, \mathbf{r}_2, \mathbf{r}'_1)] \\ & - l(\mathbf{r}_1, \mathbf{r}'_1)[P_{de}(r) - P_{de}(r') + P_{ded}(\mathbf{r}_1, \mathbf{r}_2, \mathbf{r}'_1)] - P_{cdc}(\mathbf{r}_1, \mathbf{r}_2, \mathbf{r}'_1) - P_{cdc}^2(\mathbf{r}_1, \mathbf{r}_2, \mathbf{r}'_1) \\ & - P_{cec}(\mathbf{r}_1, \mathbf{r}_2, \mathbf{r}'_1) - v[P_{cc}(r) + P_{dcc}(\mathbf{r}_1, \mathbf{r}_2, \mathbf{r}'_1)][P_{cc}(r') + P_{dcc}(\mathbf{r}'_1, \mathbf{r}_2, \mathbf{r}_1)]. \end{aligned} \quad (22)$$

The two- and three-point irreducible exchange functions $P_{\alpha\beta}$ and $P_{\alpha\beta\gamma}$ entering this expression are classified according to the presence or absence of exchange lines at the root points. The category to which a given function

$$\begin{aligned} L(\mathbf{r}_1, \mathbf{r}_2, \mathbf{r}'_1) = & -\frac{1}{v} \text{diagram} \\ & + \frac{1}{v} \left\{ \text{diagram} + \text{diagram} \right\} + \frac{1}{v} \left\{ \text{diagram} + \text{diagram} + \text{diagram} + \text{diagram} \right\} \\ & + \frac{1}{v} \left\{ \text{diagram} + \text{diagram} \right\} + \frac{1}{v} \left\{ \text{diagram} + \text{diagram} + \text{diagram} + \text{diagram} \right\} \\ & - \left\{ \text{diagram} + \text{diagram} \right\} - \left\{ \text{diagram} + \text{diagram} \right\} \\ & - \left\{ \text{diagram} + \text{diagram} \right\} \\ & - \left\{ \text{diagram} + \text{diagram} + \text{diagram} + \text{diagram} \right\} \\ & + \dots \end{aligned}$$

FIG. 9. Diagrammatic representation of the cluster expansion of the exchange function $L(\mathbf{r}_1, \mathbf{r}_2, \mathbf{r}'_1)$ (two- and three-body cluster contributions shown explicitly).

$$\begin{aligned} L_1(r) = & \text{diagram} + \text{diagram} - 2 \text{diagram} + \dots \\ L_2(r) = & - \text{diagram} + \dots \end{aligned}$$

FIG. 8. Diagrammatic representation of the cluster expansions of the exchange functions $L_1(r)$ and $L_2(r)$ (two- and three-body cluster contributions shown explicitly).

The structure of the three-point exchange function $L(\mathbf{r}_1, \mathbf{r}_2, \mathbf{r}'_1)$ cannot be determined from asymptotic properties; it is instead inferred from the cluster expansion (12) and the associated r -space representation (13) (see Figs. 5 and 6). The results through three-body cluster order are displayed diagrammatically in Fig. 9.

Inspecting Fig. 9, it is seen that many of the diagrams factorize; as the simplest example, note that the first diagram represents the product $-v^{-1}l(r)l(r')$, where $r = |\mathbf{r}_1 - \mathbf{r}_2|$ and $r' = |\mathbf{r}'_1 - \mathbf{r}_2|$. A detailed study of the three-body cluster diagrams (and selected four-body diagrams, not shown), together with a general knowledge of the nature of cluster expansions, leads one to the following structural decomposition of the three-point exchange function:

belongs is indicated by its subscripts $\alpha\beta$ or $\alpha\beta\gamma$, according to the conventional scheme:²⁰ cc (circular), de (direct exchange), dcc (direct circular), ded (direct exchange direct), cdc (circular direct circular), and cec (circular exchange circular). As usual, these functions may be separated into their nodal and elementary parts:

$$\begin{aligned} -P_{\alpha\beta}(r) = & N_{Q\alpha\beta}(r) + E_{Q\alpha\beta}(r), \\ -P_{\alpha\beta\gamma}(\mathbf{r}_1, \mathbf{r}_2, \mathbf{r}'_1) = & N_{Q\alpha\beta\gamma}(\mathbf{r}_1, \mathbf{r}_2, \mathbf{r}'_1) + E_{Q\alpha\beta\gamma}(\mathbf{r}_1, \mathbf{r}_2, \mathbf{r}'_1). \end{aligned} \quad (23)$$

The resolutions (23) parallel those asserted in (18) [the direct subscripts dd and ddd being omitted from (18) for brevity]. The leading contributions to the cluster expansion

$$\begin{aligned} N_{Qcc}(r) = & \frac{1}{v} \left\{ \text{diagram} + \text{diagram} \right\} \\ N_{Qde}(r) = & - \left\{ \text{diagram} + \text{diagram} \right\} \end{aligned}$$

FIG. 10. Diagrammatic representation of the two-body cluster contributions to the cluster expansions of the circular exchange function $N_{Qcc}(r)$ and the direct-exchange function $N_{Qde}(r)$.

$$\begin{aligned}
N_{Q_{dcc}}(\mathbf{r}_1, \mathbf{r}_2, \mathbf{r}'_1) &= \frac{1}{\nu} \left\{ \begin{array}{c} \text{diagram 1} \\ \text{diagram 2} \\ \text{diagram 3} \\ \text{diagram 4} \end{array} \right\} \\
N_{Q_{ded}}(\mathbf{r}_1, \mathbf{r}_2, \mathbf{r}'_1) &= - \left\{ \begin{array}{c} \text{diagram 5} \\ \text{diagram 6} \end{array} \right\} \\
N_{Q_{cdc}}(\mathbf{r}_1, \mathbf{r}_2, \mathbf{r}'_1) &= - \left\{ \begin{array}{c} \text{diagram 7} \\ \text{diagram 8} \\ \text{diagram 9} \\ \text{diagram 10} \end{array} \right\}
\end{aligned}$$

FIG. 11. Diagrammatic representation of the three-body cluster contributions to the cluster expansions of the irreducible three-point functions $N_{Q_{dcc}}(\mathbf{r}_1, \mathbf{r}_2, \mathbf{r}'_1)$, $N_{Q_{ded}}(\mathbf{r}_1, \mathbf{r}_2, \mathbf{r}'_1)$, and $N_{Q_{cdc}}(\mathbf{r}_1, \mathbf{r}_2, \mathbf{r}'_1)$.

sions of the $P_{\alpha\beta}$ and $P_{\alpha\beta\gamma}$ (or equivalently the $N_{Q_{\alpha\beta}}$ and $N_{Q_{\alpha\beta\gamma}}$, since the elementary diagrams are of higher order) are depicted in Figs. 10–12. The two-point functions $P_{\alpha\beta}$ arise already in the theory of the one-body density matrix and may therefore be regarded as known quantities; their structure has been thoroughly investigated within the FHNC formalism.^{15,16} They may be calculated to all cluster orders by solving a coupled set of FHNC integral equations.¹⁶ In FHNC/0 approximation, elementary contributions are neglected, so the three-point functions $P_{\alpha\beta\gamma}$ are approximated by their nodal portions $N_{Q_{\alpha\beta\gamma}}$. Since our initial numerical investigation is carried out at the FHNC/0 level, we do not give explicit representations of the various elementary contributions. They may be constructed in a straightforward manner as the need arises in subsequent, more elaborate numerical calculations with scaling or interpolation schemes.^{24–28}

It is instructive to specialize our structural results to the case $\mathbf{r}_1 = \mathbf{r}'_1$. The matrix elements $\rho_2(\mathbf{r}_1, \mathbf{r}_2, \mathbf{r}_1)$ must reproduce the radial distribution function $g(r)$ according to

$$\rho_2(\mathbf{r}_1, \mathbf{r}_2, \mathbf{r}_1) = \rho^2 g(r). \quad (24)$$

For the assumed wave function (6), the structure of $g(r)$ was established at the very beginning of FHNC theory. Explicitly, $g(r)$ takes the form²⁰

$$\begin{aligned}
N_{Q_{ccc}}(\mathbf{r}_1, \mathbf{r}_2, \mathbf{r}'_1) &= \left\{ \begin{array}{c} \text{diagram 11} \\ \text{diagram 12} \\ \text{diagram 13} \\ \text{diagram 14} \end{array} \right. \\
&+ \left. \begin{array}{c} \text{diagram 15} \\ \text{diagram 16} \\ \text{diagram 17} \\ \text{diagram 18} \end{array} \right\} \\
&+ 2 \left\{ \begin{array}{c} \text{diagram 19} \\ \text{diagram 20} \\ \text{diagram 21} \\ \text{diagram 22} \end{array} \right\} \\
&+ \left\{ \begin{array}{c} \text{diagram 23} \\ \text{diagram 24} \\ \text{diagram 25} \\ \text{diagram 26} \end{array} \right\}
\end{aligned}$$

FIG. 12. Diagrammatic representation of the four-body cluster contributions to the cluster expansion of the irreducible three-point function $N_{Q_{ccc}}(\mathbf{r}_1, \mathbf{r}_2, \mathbf{r}'_1)$.

$$\begin{aligned}
g(r) &= f^2(r) \exp[N_{dd}(r) + E_{dd}(r)] \\
&\times \{ 1 - \nu^{-1} l^2(r) + 2l(r)[N_{cc}(r) + E_{cc}(r)] \\
&\quad + 2[N_{de}(r) + E_{de}(r)] + [N_{de}(r) + E_{de}(r)]^2 \\
&\quad + [N_{ee}(r) + E_{ee}(r)] - \nu[N_{cc}(r) + E_{cc}(r)]^2 \}. \quad (25)
\end{aligned}$$

At $\mathbf{r}_1 = \mathbf{r}'_1$, the results (15), (16), (17), and (21), together with the property¹⁴ $L_1(\mathbf{r}_1, \mathbf{r}_1) + L_2(\mathbf{r}_1, \mathbf{r}_1) = 1$, yield

$$\begin{aligned}
\rho_2(\mathbf{r}_1, \mathbf{r}_2, \mathbf{r}_1) &= \rho^2 f^2(r) \{ \exp[-2P(r) - P(\mathbf{r}_1, \mathbf{r}_2, \mathbf{r}_1)] \\
&\quad \times [1 + L(\mathbf{r}_1, \mathbf{r}_2, \mathbf{r}_1)] \}. \quad (26)
\end{aligned}$$

In Ref. 7 it was shown that for the Bose fluid, the exponential expression in (26) reduces to

$$-2P(r) - P(\mathbf{r}_1, \mathbf{r}_2, \mathbf{r}_1) = N_{dd}(r) + E_{dd}(r), \quad (27)$$

where $N_{dd}(r)$ and $E_{dd}(r)$ are—as required for (24) to hold—the nodal and elementary diagram sums that generate the radial distribution function. (Again, the direct subscripts dd and ddd are understood in the Bose case, and therefore omitted in Ref. 7.) Relation (27) also holds for the Fermi fluid, provided the functions $N_{dd}(r)$ and $E_{dd}(r)$ are interpreted as the direct-direct nodal and elementary generating functions involved in Eq. (25). (We stress that these diagram sums differ from their Bose counterparts by the presence of extra diagrams having exchange lines at field points.) Specializing the irreducible exchange quantities among $P_{\alpha\beta}(r)$ and $P_{\alpha\beta\gamma}(\mathbf{r}_1, \mathbf{r}_2, \mathbf{r}'_1)$ [which define the structural decomposition (22)] to the case $\mathbf{r}_1 = \mathbf{r}'_1$, we obtain the analogous relations

$$\begin{aligned}
-P_{cc}(r) - P_{dcc}(\mathbf{r}_1, \mathbf{r}_2, \mathbf{r}_1) &= N_{cc}(r) + E_{cc}(r), \\
-2P_{de}(r) - P_{ded}(\mathbf{r}_1, \mathbf{r}_2, \mathbf{r}_1) &= N_{de}(r) + E_{de}(r), \\
-P_{cdc}(\mathbf{r}_1, \mathbf{r}_2, \mathbf{r}_1) &= N_{de}(r) + E_{de}(r), \\
-P_{cec}(\mathbf{r}_1, \mathbf{r}_2, \mathbf{r}_1) &= N_{ee}(r) + E_{ee}(r). \quad (28)
\end{aligned}$$

The nodal and elementary diagram sums on the right-hand side are just those (with corresponding subscripts) which arise in the FHNC analysis of the radial distribution function [cf. Eq. (25) and Ref. 20]. Insertion of (28) into (26), via (22), completes the desired connection (24).

To conclude this section, we point out that the relations (28) provide the basis for a simple recipe for constructing the elementary three-point functions $E_{Q_{\alpha\beta\gamma}}(\mathbf{r}_1, \mathbf{r}_2, \mathbf{r}'_1)$ from the corresponding elementary two-point functions appearing on the right-hand side, which may be considered as known quantities. The dynamical and/or exchange bonds ending at the root point \mathbf{r}_1 of contributions to a given two-point function are to be properly opened up to yield contributions to a three-point function with the three distinct root points $\mathbf{r}_1, \mathbf{r}_2, \mathbf{r}'_1$.

IV. FORM FACTORS

We next explore the structure of the generalized momentum distribution function $n(\mathbf{p}, \mathbf{q})$ of (2) by implementing the structural results (15), (16), (17), (21), and

(22) for the two-body density-matrix elements $\rho_2(\mathbf{r}_1, \mathbf{r}_2, \mathbf{r}'_1)$ appearing in the integral (14). To obtain a decomposition of $n(\mathbf{p}, \mathbf{q})$ that separates contributions from differing physical processes in a clean manner, the function $\rho_2(\mathbf{r}_1, \mathbf{r}_2, \mathbf{r}'_1)$ is first split up into a portion containing all terms generated purely by two-point functions, and a remainder in which the terms also depend on the irreducible three point functions. Thus

$$\rho_2(\mathbf{r}_1, \mathbf{r}_2, \mathbf{r}'_1) = \rho_2^{(2)}(\mathbf{r}_1, \mathbf{r}_2, \mathbf{r}'_1) + \rho_2^{(3)}(\mathbf{r}_1, \mathbf{r}_2, \mathbf{r}'_1), \quad (29)$$

in an obvious notation. The last term vanishes if we set the various three-point functions $P(\mathbf{r}_1, \mathbf{r}_2, \mathbf{r}'_1)$ and $P_{\alpha\beta\gamma}(\mathbf{r}_1, \mathbf{r}_2, \mathbf{r}'_1)$ equal to zero.

Secondly, we invoke the Fermi-hypernet equations resulting from the FHNC analysis of the one-body density matrix.^{15,16} These equations relate the bare correlation function $f(r)$ to the spatial distribution functions defined by the non-nodal and nodal diagram sums $X_{Q\alpha\beta}(r)$ and $N_{Q\alpha\beta}(r)$ introduced in Refs. 15 and 16:

$$\begin{aligned} g_{Qdd}(r) &= 1 + F_{dd}(r) = 1 + X_{Qdd}(r) + N_{Qdd}(r), \\ g_{Qcc}(r) &= 1 + F_{cc}(r) = 1 + X_{Qcc}(r) + N_{Qcc}(r), \\ g_{Qde}(r) &= 1 + F_{de}(r) = 1 + X_{Qde}(r) + N_{Qde}(r). \end{aligned} \quad (30)$$

$$\begin{aligned} \rho_2^{(2)}(\mathbf{r}_1, \mathbf{r}_2, \mathbf{r}'_1) &= \rho\rho_1(\mathbf{r}_1, \mathbf{r}'_1)g_{Qdd}(r)g_{Qdd}(r') + \rho\rho_{1D}(\mathbf{r}_1, \mathbf{r}'_1)l(\mathbf{r}_1, \mathbf{r}'_1)[g_{Qdd}(r)F_{de}(r') + g_{Qdd}(r')F_{de}(r)] \\ &\quad - \nu\rho\rho_{1D}(\mathbf{r}_1, \mathbf{r}'_1)[\nu^{-1}l(r) - F_{cc}(r)][\nu^{-1}l(r') - F_{cc}(r')] \end{aligned} \quad (32)$$

and

$$\begin{aligned} \rho_2^{(3)}(\mathbf{r}_1, \mathbf{r}_2, \mathbf{r}'_1) &= \rho_2^{(2)}(\mathbf{r}_1, \mathbf{r}_2, \mathbf{r}'_1)\{\exp[-P(\mathbf{r}_1, \mathbf{r}_2, \mathbf{r}'_1)] - 1\} \\ &\quad + \rho\rho_{1D}(\mathbf{r}_1, \mathbf{r}'_1)g_{Qdd}(r)g_{Qdd}(r')\exp[-P(\mathbf{r}_1, \mathbf{r}_2, \mathbf{r}'_1)] \\ &\quad \times [-l(r)P_{dcc}(\mathbf{r}'_1, \mathbf{r}_2, \mathbf{r}_1) - l(r')P_{dcc}(\mathbf{r}_1, \mathbf{r}_2, \mathbf{r}'_1) - l(\mathbf{r}_1, \mathbf{r}'_1)P_{ded}(\mathbf{r}_1, \mathbf{r}_2, \mathbf{r}'_1) \\ &\quad - P_{cdc}(\mathbf{r}_1, \mathbf{r}_2, \mathbf{r}'_1) + P_{cdc}^2(\mathbf{r}_1, \mathbf{r}_2, \mathbf{r}'_1) - P_{ccc}(\mathbf{r}_1, \mathbf{r}_2, \mathbf{r}'_1) - \nu P_{dcc}(\mathbf{r}_1, \mathbf{r}_2, \mathbf{r}'_1)P_{dcc}(\mathbf{r}'_1, \mathbf{r}_2, \mathbf{r}_1) \\ &\quad - \nu P_{cc}(r)P_{dcc}(\mathbf{r}'_1, \mathbf{r}_2, \mathbf{r}_1) - \nu P_{cc}(r')P_{dcc}(\mathbf{r}_1, \mathbf{r}_2, \mathbf{r}'_1)], \end{aligned} \quad (33)$$

where, as before, $r = |\mathbf{r}_1 - \mathbf{r}_2|$ and $r' = |\mathbf{r}'_1 - \mathbf{r}_2|$.

Inserting (29) into the integral (14), and utilizing the results (32) and (33), we arrive at the decomposition

$$\begin{aligned} n(\mathbf{p}, \mathbf{q}) &= N\delta_{q0}n(p) + F_{dd}(q)[n(p) + n(|\mathbf{p} - \mathbf{q}|)] + F_{de}(q)[n_{Dl}(p) + n_{Dl}(|\mathbf{p} - \mathbf{q}|)] \\ &\quad - n_0[\Theta(k_F - p) - F_{cc}(p)][\Theta(k_F - |\mathbf{p} - \mathbf{q}|) - F_{cc}(|\mathbf{p} - \mathbf{q}|)] + n^{(2)'}(\mathbf{p}, \mathbf{q}) + n^{(3)'}(\mathbf{p}, \mathbf{q}). \end{aligned} \quad (34)$$

Thus the component $n(\mathbf{p}, \mathbf{q}) - N\delta_{q0}n(p)$ of the generalized momentum distribution is expressed as a sum of (i) separable contributions involving form factors

$$F_{\alpha\beta}(q) = \rho \int F_{\alpha\beta}(r) e^{iq \cdot r} d\mathbf{r} \quad (35)$$

and either the one-body momentum distribution (1), a modified momentum distribution

$$n_{Dl}(p) = \nu^{-1} \int \rho_{1D}(r) l(r) e^{ip \cdot r} d\mathbf{r}, \quad (36)$$

or the strength factor n_0 [second, third, and fourth terms of (34), respectively]; (ii) a nonseparable integral $n^{(2)'}(\mathbf{p}, \mathbf{q})$ involving only two-point quantities; and (iii) another three-point integral $n^{(3)'}(\mathbf{p}, \mathbf{q})$ generated from the component (33) of $\rho_2(\mathbf{r}_1, \mathbf{r}_2, \mathbf{r}'_1)$. Explicitly, the fifth term is

$$n^{(2)'}(\mathbf{p}, \mathbf{q}) = \frac{1}{\nu} \frac{\rho}{N} \int K(\mathbf{r}_1, \mathbf{r}_2, \mathbf{r}'_1) e^{-i\mathbf{p} \cdot (\mathbf{r}_1 - \mathbf{r}'_1)} e^{-i\mathbf{q} \cdot (\mathbf{r}_1 - \mathbf{r}_2)} d\mathbf{r}_1 d\mathbf{r}_2 d\mathbf{r}'_1, \quad (37)$$

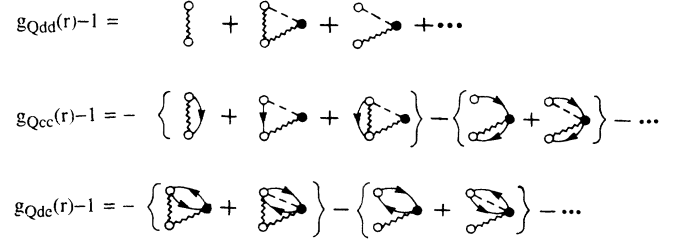


FIG. 13. Diagrammatic representation of the cluster expansions of the spatial distribution functions $g_{Qdd}(r)$, $g_{Qcc}(r)$, and $g_{Qde}(r)$ (two- and three-body cluster contributions shown explicitly).

Figure 13 indicates the diagrammatic structure of these quantities, in leading cluster approximations. Having established the necessary notation, the hypernet equations read

$$\begin{aligned} f(r) e^{-P(r)} &= g_{Qdd}(r), \\ -f(r) e^{-P(r)} P_{cc}(r) &= \nu^{-1} l(r) F_{dd}(r) + F_{cc}(r), \\ -f(r) e^{-P(r)} P_{de}(r) &= F_{de}(r). \end{aligned} \quad (31)$$

Equations (31) are used to eliminate the bare correlation factor $f(r)$ from each term of the explicit expression for the decomposition (29). These manipulations produce

where

$$K(\mathbf{r}_1, \mathbf{r}_2, \mathbf{r}'_1) = \rho \rho_1(\mathbf{r}_1, \mathbf{r}'_1) F_{Qdd}(r) F_{Qdd}(r') + \rho \rho_{1D}(\mathbf{r}_1, \mathbf{r}'_1) l(\mathbf{r}_1, \mathbf{r}'_1) [F_{Qdd}(r) F_{de}(r') + F_{Qdd}(r') F_{de}(r)] - \nu \rho [\rho_{1D}(\mathbf{r}_1, \mathbf{r}'_1) - \rho n_0] [\nu^{-1} l(r) - F_{cc}(r)] [\nu^{-1} l(r') - F_{cc}(r')] . \quad (38)$$

Inserting the Fourier inverses of the two-point functions F_{Qdd} , etc., appearing in $K(\mathbf{r}_1, \mathbf{r}_2, \mathbf{r}'_1)$, while recalling that $\rho_1(\mathbf{r}_1, \mathbf{r}'_1)$, $\rho_{1D}(\mathbf{r}_1, \mathbf{r}'_1)$, and $l(\mathbf{r}_1, \mathbf{r}'_1)$ depend only on $|\mathbf{r}_1 - \mathbf{r}'_1|$, we may convert (37) into a three-dimensional integral in momentum variables.

Appealing to the sequential relation¹⁹

$$\int \rho_2(\mathbf{r}_1, \mathbf{r}_2, \mathbf{r}'_1) d\mathbf{r}_2 = (N-1) \rho_1(\mathbf{r}_1, \mathbf{r}'_1) , \quad (39)$$

the intermediate result (34) may be recast in a preferable form. In momentum space, the sequential condition becomes

$$n(\mathbf{p}, \mathbf{q}=0) = (N-1)n(p) . \quad (40)$$

We specialize (34) to $\mathbf{q}=0$ and compare with (40). The condition for equivalence is then framed as a condition on the form factors entering (34):

$$[1 + 2F_{dd}(0)]n(p) + 2F_{de}(0)n_{Dl}(p) + n^{(2)' }(\mathbf{p}, 0) + n^{(3)' }(\mathbf{p}, 0) = n_0 [\Theta(k_F - p) - F_{cc}(p)]^2 . \quad (41)$$

Assuming that (41) is fulfilled, we may employ it to rewrite (34) in the form

$$n(\mathbf{p}, \mathbf{q}) = (N-1)\delta_{q0}n(p) + (1-\delta_{q0})F_{dd}(q)[n(p) + n(|\mathbf{p}-\mathbf{q}|)] + (1-\delta_{q0})F_{de}(q)[n_{Dl}(p) + n_{Dl}(|\mathbf{p}-\mathbf{q}|)] - n_0(1-\delta_{q0})[\Theta(k_F - p) - F_{cc}(p)][\Theta(k_F - |\mathbf{p}-\mathbf{q}|) - F_{cc}(|\mathbf{p}-\mathbf{q}|)] + (1-\delta_{q0})n^{(2)' }(\mathbf{p}, \mathbf{q}) + (1-\delta_{q0})n^{(3)' }(\mathbf{p}, \mathbf{q}) . \quad (42)$$

This expression achieves the desired separation of contributions from the various scattering processes underlying the generalized momentum distribution function (cf. Ref. 7). The first term reproduces the result (4) for dynamically and kinematically uncorrelated fermions [except that the dressed momentum distribution function $n(p)$ must be used]. The correlations prevailing in the interacting fluid permit the scattering of a fermion from orbital $\hat{\mathbf{p}}$ to another orbital $\hat{\mathbf{p}} - \mathbf{q}$, with the intervention of a phonon to conserve momentum. The effect of this process and the corresponding time-reversed process are described by the second term in (42). The associated exchange scattering effects are embodied in the third term, which is proportional to the exchange form factor $F_{de}(q)$ depending on the phonon wave number q . The fourth term of (42) is recognized as the dressed version of the kinematic (Pauli) correlation effect introduced in Eq. (5). In the present case, the dynamical correlations, manifested in virtual excitations of fermions above the Fermi surface, lead to tails on the step distributions (the F_{cc} terms). The dynamical correlations also produce an overall quenching of the effect, through the strength factor n_0 ($0 \leq n_0 \leq 1$). The last two addends of (42) are terms of "higher order," which act to correct the various processes just considered.

By taking the Bose limit ($\nu \rightarrow \infty, k_F \rightarrow 0+, \rho$ fixed), we may recover the corresponding decomposition of the generalized momentum distribution of a Bose fluid as reported in Ref. 7. Only the direct contributions to (42) survive. Thus the third and fourth terms are to be omitted, and the form factor $F_{dd}(q)$ is to be identified with the function $F_1(q)$ studied in the earlier paper.

At this point, a useful remark about condition (41) is in order. In the Bose limit, we may split this relation into

two conditions, one applying at $p=0$ (the condensate condition) and the other applying at finite p (and involving terms smaller by a factor $1/N$). These conditions read, respectively, $1 + 2F_1(0) = 0$ and $n^{(2)' }(\mathbf{p}, 0) + n^{(3)' }(\mathbf{p}, 0) = 0$, in agreement with what was found in Ref. 7. As discussed in Ref. 7, these conditions constrain the choice of correlation factor in the Bose case. In the Fermi case, the situation is different: It may be shown that the sequential relation expressed in (41) is fulfilled identically for *any* Jastrow trial function (6), and indeed, even if this choice is extended to include multibody correlations of Feenberg type.²² The automatic satisfaction of (41) is a consequence of the presence of Pauli exchange correlations, implied by the Slater determinant Φ . Technically, this property may be attributed to a Fermi cancellation phenomenon of the type encountered in the FHNC analysis of the static structure function $S(q)$ (see Refs. 29 and 20 for details).

V. NUMERICAL RESULTS

In calculating final-state corrections of the impulse approximation to deep-inelastic scattering from the helium liquids, Silver²⁻⁵ has employed the simple approximation

$$\rho_2(\mathbf{r}_1, \mathbf{r}_2, \mathbf{r}'_1) \simeq \rho \rho_1(\mathbf{r}_1, \mathbf{r}'_1) g(|\mathbf{r}_1 - \mathbf{r}_2|) \quad (43)$$

for the relevant two-body density-matrix elements. We may test the quality of this assumption by evaluating the functions $\rho_2(\mathbf{r}_1, \mathbf{r}_2, \mathbf{r}'_1)$, $\rho_1(\mathbf{r}_1, \mathbf{r}'_1)$, and $g(r)$, and the associated momentum distributions and structure functions, within the microscopic treatment developed in the preceding sections. Such a test was carried out for the Bose case in Ref. 7, where numerical results were presented in HNC/0 approximation and some steps for sys-

tematic improvement on the estimate (43) were indicated. Here we repeat the process for the Fermi problem, where Pauli exchange effects must be adequately included.

We may view Silver's approximation (43) as arising from rough first estimates of quantities in the contributions (32) and (33) to the expression (29) en route to the result (42). In more detail, it amounts to a truncation of (32) corresponding to the replacements

$$\rho_1(\mathbf{r}_1, \mathbf{r}'_1) \approx \rho_{1D}(\mathbf{r}_1, \mathbf{r}'_1) l(\mathbf{r}_1, \mathbf{r}'_1), \quad (44)$$

$$F_{dd}(r') \approx 0, \quad F_{de}(r') \approx 0 \quad (45)$$

$$1 + F_{dd}(r) + F_{de}(r) \approx g(r), \quad (46)$$

$$v^{-1} l(r') - F_{cc}(r') \approx 0, \quad (47)$$

and to the neglect of the "pure-three-point" contribution $\rho_2^{(3)}(\mathbf{r}_1, \mathbf{r}_2, \mathbf{r}'_1)$ of Eq. (33). In momentum space, the replacements (44), (46), and (47) translate, respectively, to

$$n(p) \approx n_{DI}(p), \quad (48)$$

$$F_{dd}(q) + F_{de}(q) \approx S(q) - 1, \quad (49)$$

and

$$\Theta(k_F - p) - F_{cc}(p) \approx 0, \quad (50)$$

where $S(q)$ is the static structure function corresponding to the radial distribution function $g(r)$.

The most striking feature of Silver's approximation is, of course, its violation of time-reversal invariance, evident in the asymmetric treatment of at least one of the pairs $F_{dd}(r), F_{dd}(r')$ and $F_{de}(r), F_{de}(r')$ by Eqs. (45) and (46).

To make a quantitative assessment of the merit of approximations (44)–(47), we have used the microscopic formalism developed in Secs. II–IV to calculate the various functions appearing in these relations, for the specific case of liquid ${}^3\text{He}$ at equilibrium density, $\rho = 0.01658 \text{ \AA}^{-3}$. The trial ground state is of the Jastrow-Slater form (6), with the Schiff-Verlet choice¹⁷ $f(r) = \exp[-(b/r)^5/2]$ for the two-body correlation function. As in Ref. 18, we take $b = 2.9547 \text{ \AA}$. The density matrices $\rho_1(\mathbf{r}_1, \mathbf{r}'_1), \rho_2(\mathbf{r}_1, \mathbf{r}_2, \mathbf{r}'_1)$, the distribution functions $n(p), n_{DI}(p)$, and the various form factors $F_{dd}(q), F_{de}(q), F_{cc}(q)$ are evaluated in FHNC/0 approximation, ignoring contributions from elementary diagrams.

In a next step, one should invoke a scaling or interpolation procedure^{24–28} for the incorporation of elementary corrections. Numerical work in this direction is in progress.³⁰ Although technically involved, this extension does not pose any serious difficulties.

Figures 14–16 summarize the results at the FHNC/0 level, which should be accurate enough for the immediate task of judging approximation (43) through its ingredients (44)–(50). The momentum distribution functions $n(p)$ and $n_{DI}(p)$ involved in the assumed relation (48) are compared in Fig. 14. The strength factor associated with both of these functions is $n_0 = 0.2212$. The two functions are seen to have very similar behavior, but their magnitudes differ typically by 10–15%. Figure 15 pro-

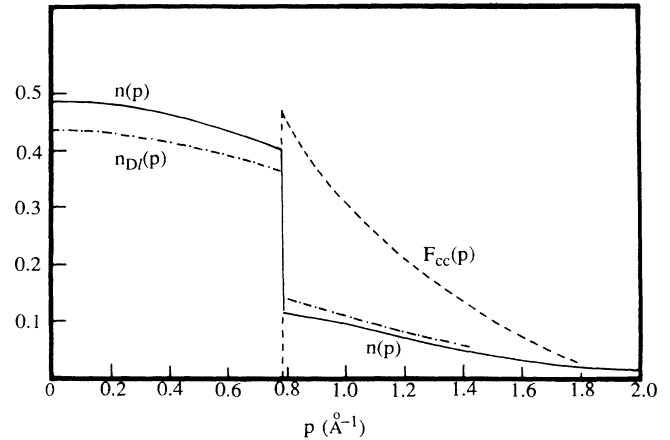


FIG. 14. Momentum distribution functions $n(p)$ (solid curve) and $n_{DI}(p)$ (dot-dashed curve) of liquid ${}^3\text{He}$ at density $\rho = 0.01658 \text{ \AA}^{-3}$. The calculation is based on ansatz (6) with a correlation factor $f(r)$ of Schiff-Verlet type and employs the FHNC/0 approximation. The dashed curve is the circular-exchange function $F_{cc}(p)$ [cf. Silver's relations (48) and (50)].

vides a comparison of the numerical results for $g(r) - 1$ and $F_{dd}(r) + F_{de}(r)$ and thus tests the assumption (46). Generally speaking, the situation is similar to that found in our earlier HNC/0 study of the Bose fluid:⁷ These two functions have much the same shape, but quantitatively they differ significantly.

The poor quality of the estimate (46) is revealed more vividly in Fig. 16, which shows $S(q) - 1$ and the sum of form factors $F_{dd}(q) + F_{de}(q)$. The strong deviation from assumption (49) is clearly exposed and is particularly apparent at small momenta. The corresponding behavior was noted for the Bose case in Ref. 7. For a Bose fluid, $1 - S(q)$ approaches unity as q goes to zero, while the function $F_1(q)$ [or $F_{dd}(q)$, the exchange form factor $F_{ee}(q)$ being absent] goes to $-\frac{1}{2}$. The exclusion principle, and the Fermi cancellation effect pointed out in Sec. IV,

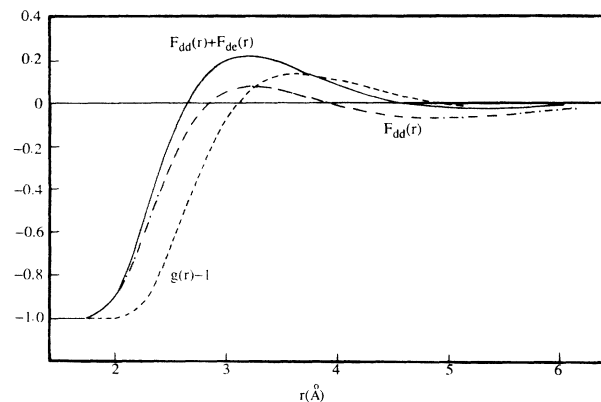


FIG. 15. Comparison of the function $F_{dd}(r) + F_{de}(r)$ (solid curve) and the radial distribution function $g(r)$ (with unity subtracted, dashed curve) for liquid ${}^3\text{He}$, based on the Jastrow-FHNC/0 approximation. The dot-dashed curve is the direct-direct portion $F_{dd}(r)$ [cf. Silver's relation (46)].

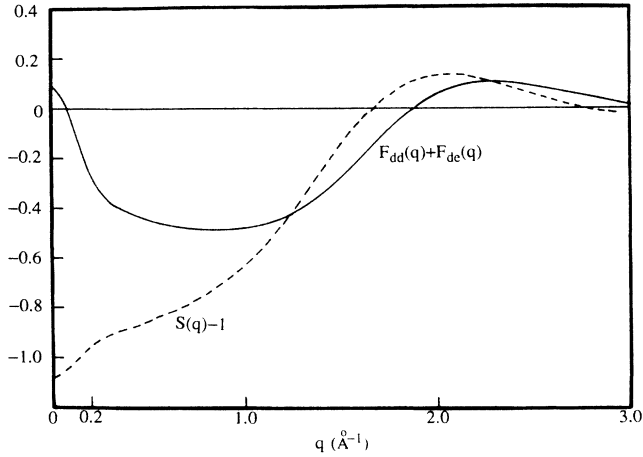


FIG. 16. Sum of form factors $F_{dd}(q) + F_{de}(q)$ (solid curve) compared with the static structure function $S(q)$ (minus unity, dashed curve), for liquid ^3He as described within the Jastrow-FHNC/0 approximation [cf. Silver's relation (49)].

alter this picture. For a Fermi system described by the wave function (6), this cancellation phenomenon guarantees, at $q=0$, the behavior $X_{de}(q) = X_{ee}(q) = -1$ and, consequently, $S(q) = 0$ and $F_{dd}(q) + F_{de}(q) = 0$. The latter properties are (approximately) reflected in our numerical results for $S(q)$ and $F_{dd}(q) + F_{de}(q)$. However, one does see, in Fig. 16, slight deviations from the correct limiting values, which result from use of the FHNC/0 approximation. The standard FHNC approximants (/0, /4, etc.) are known to disobey the Fermi cancellation rules as a result of the neglect or inconsistent treatment of elementary diagrams.²⁰

The Pauli exclusion corrections to $n(\mathbf{p}, \mathbf{q})$ of the circular type, involving $\Theta(k_F - p) - F_{cc}(p)$, are entirely ignored in Silver's treatment—even the trivial kinematic statistical effect of the first term is absent. The form factor $F_{cc}(p)$, evaluated in FHNC/0 approximation, is shown in Fig. 14 as the dashed line. This function vanishes inside the Fermi sea, jumps to a height of about 0.5 at the Fermi surface, and decreases slowly in magnitude with further increase of the wave number p . In general one may therefore expect such statistical effects to be important. On the other hand, we note that their net contribution to $n(\mathbf{p}, \mathbf{q})$ of (42) is proportional to the strength factor n_0 , which is only about 0.2 in liquid ^3He .

At this stage, we shall not report numerical data on the contributions $n^{(2')}(\mathbf{p}, \mathbf{q})$ and $n^{(3')}(\mathbf{p}, \mathbf{q})$ to $n(\mathbf{p}, \mathbf{q})$ as expressed in (42). They may be calculated from quantities generated in the FHNC/0 treatment, by performing a series of integrations. It must be recognized, however, that within the FHNC/0 framework the sequential relation (39) is not fulfilled because of the neglect of elementary diagrams. This shortcoming of the FHNC/0 approximation may be adequately corrected by implementation of a suitable scaling or interpolation scheme.²⁴⁻²⁸ Accordingly, we postpone a detailed assessment of $n^{(2')}$ and $n^{(3')}$ until such an improved numerical evaluation has been completed.

In summary, an initial application of the microscopic theory of the density-matrix elements $\rho_2(\mathbf{r}_1, \mathbf{r}_2, \mathbf{r}'_1)$ has uncovered significant quantitative deficiencies of the simple estimate proposed by Silver. On the other hand, it remains to be determined whether or not these deficiencies have serious consequences in the treatment of final-state corrections to deep-inelastic scattering within Silver's theory. In the case of neutron scattering from liquid ^4He , predictions of the latter theory based on (43) are in excellent agreement with the Compton profile measured at momentum transfer $Q = 23 \text{ \AA}^{-1}$ (Ref. 6). The degree of agreement might be taken as evidence that the final-state modifications at high momentum and energy transfers are insensitive to the errors we have noted, and, in particular, to the small- q behavior of the Bose form factor $F_{dd}(q)$ appropriate to liquid ^4He . However, this conclusion is subject to question because there are many approximations entering Silver's analysis, including the neglect of corrections $O(1/Q)$. To decide this issue, we have undertaken a quantitative reevaluation of the predictions of Silver's theory, using the methods developed in Ref. 7 and the present article for the computation of the required two-body density matrix elements. The results will be the subject of a future paper.

ACKNOWLEDGMENTS

This research was supported in part by the Comision de Investigacion Cientifica y Tecnica, Spain (CICYT) and by the Condensed Matter Theory Program of the Division of Materials Research of the U.S. National Science Foundation, under Grant No. DMR-8519077. M.L.R. enjoyed the hospitality of the Departamento de Fisica Moderna, Universidad de Granada, and the

$$\begin{aligned}
 (17.1) \quad & \text{---} \circ \text{---} \circ = f(\mathbf{r}_1, \mathbf{r}'_1) - 1 = \zeta(|\mathbf{r}_1 - \mathbf{r}'_1|) \\
 (17.2) \quad & \text{---} \circ \text{---} \circ = f^2(\mathbf{r}_1, \mathbf{r}'_1) - 1 = \eta(|\mathbf{r}_1 - \mathbf{r}'_1|) \\
 (17.3) \quad & \text{---} \circ \text{---} \circ = l(|\mathbf{r}_1 - \mathbf{r}'_1|) \equiv l(x) = 3x^{-3}(\sin x - x \cos x) \\
 (17.4) \quad & \text{---} \circ \text{---} \circ = e^{-i\mathbf{p} \cdot (\mathbf{r}_1 - \mathbf{r}'_1)} \\
 (17.5) \quad & \begin{array}{c} \uparrow \mathbf{r}_2 \\ \text{---} \circ \\ \text{---} \circ \\ \uparrow \mathbf{r}_1 \end{array} = e^{-i\mathbf{q} \cdot (\mathbf{r}_1 - \mathbf{r}_2)} \\
 (17.6) \quad & \text{---} \circ \text{---} \circ \quad (17.7) \quad \text{---} \circ \text{---} \circ \\
 (17.8) \quad & \text{---} \circ \text{---} \circ \quad (17.9) \quad \text{---} \circ \text{---} \circ
 \end{aligned}$$

FIG. 17. Elements of the diagrammatic representation of cluster contributions in the variational description of a uniform Fermi fluid.

Department of Physics, Washington University, during leave from the Institut für Theoretische Physik, Universität zu Köln J.W.C. thanks the Theoretical Physics Institute of the University of Minnesota for financial support and gracious hospitality during the completion of this work. We are indebted to Fernando Arias de Saavedra and Enrique Buendia for furnishing the numerical data for our analysis, and we have benefited from many informative discussions with R. N. Silver.

APPENDIX

The elements of the Ursell-Mayer diagrammatic representation, adapted to a Fermi system described by a Slater-Jastrow wave function, consist of *root* (or reference, or external) *points*, *field* (or internal) *points*, *direct bonds*, *exchange bonds*, *plane waves*, and *degeneracy factors*. Figure 17 serves as a key.

A *root point* represents a particle coordinate, say \mathbf{r}_1 , which is not integrated over, whereas a *field point*, say \mathbf{r}_f , implies an integration $\int d\mathbf{r}_f$ and a density factor ρ . In the diagrams of this paper, root points are indicated by open circles with the implicit labels \mathbf{r}_1 , \mathbf{r}_2 , and \mathbf{r}'_1 , while

field points are drawn as solid dots. The bottom left open circle is identified with \mathbf{r}_1 , the bottom right with \mathbf{r}'_1 , and the top open circle with \mathbf{r}_2 .

Bonds representing dynamical and statistical correlations join pairs of coordinate points. As shown in diagrams (17.1) and (17.2), the dynamical *direct bonds* are wavy or dashed lines. An *exchange bond* is a solid line bearing an arrow, as in diagram (17.3); note that the direction of the arrow is actually immaterial. A *plane-wave bond*, as in diagram (17.4) or (17.5), also consists of a solid line with an arrow, but the line extends beyond the coordinate points on either side. The analytic counterparts of wavy-direct, dashed-direct, plane-wave, and exchange bonds joining points \mathbf{r}_i and \mathbf{r}_j are, respectively, $\zeta(r_{ij})=f(r_{ij})-1$, $\eta(r_{ij})=f^2(r_{ij})-1$, $\exp(i\mathbf{p}\cdot\mathbf{r}_{ij})$, and $l(k_F r_{ij})$, where $\mathbf{r}_{ij}=\mathbf{r}_i-\mathbf{r}_j$, $r_{ij}=|\mathbf{r}_{ij}|$, and $l(x)=3x^{-3}(\sin x - x \cos x)$.

Chains of exchange bonds connecting coordinate points introduce factors ν^{-1} , where ν is the single-particle level degeneracy. Precise rules are given in Refs. 14, 20, and 31; in particular, a closed loop of exchange lines joining m fields points contributes a factor ν^{1-m} .

The application of the diagram rules is illustrated by the following examples:

$$\text{diagram (17.6)}=l(\mathbf{r}_1,\mathbf{r}_2)l(\mathbf{r}'_1,\mathbf{r}_2),$$

$$\text{diagram (17.7)}=\frac{\rho}{\nu} \int d\mathbf{r}_2 l(\mathbf{r}_1,\mathbf{r}_2)l(\mathbf{r}_2,\mathbf{r}'_1)=l(\mathbf{r}_1,\mathbf{r}'_1) \quad (17.3),$$

$$\text{diagram (17.8)}=\frac{\rho}{\nu} \int d\mathbf{r}_3 \zeta(\mathbf{r}_1,\mathbf{r}_3)l(\mathbf{r}_1,\mathbf{r}_3)l(\mathbf{r}_3,\mathbf{r}_2)l(\mathbf{r}_2,\mathbf{r}'_1),$$

$$\text{diagram (17.9)}=\left[\frac{\rho}{\nu}\right]^2 \int d\mathbf{r}'_1, d\mathbf{r}_2 \zeta(\mathbf{r}_1,\mathbf{r}_2)l(\mathbf{r}_1,\mathbf{r}_2)l(\mathbf{r}_2,\mathbf{r}'_1) e^{-i\mathbf{p}\cdot(\mathbf{r}_1-\mathbf{r}'_1)} e^{-i\mathbf{q}\cdot(\mathbf{r}'_1-\mathbf{r}_2)}.$$

The second line asserts an important convolution property of exchange lines.

¹P. C. Hohenberg and P. M. Platzman, Phys. Rev. **152**, 198 (1966).

²R. N. Silver, in *Condensed Matter Theories*, edited by J. S. Arponen, R. F. Bishop, and M. Manninen (Plenum, New York, 1988), Vol. 3, p. 131; in *Condensed Matter Theories*, edited by J. Keller (Plenum, New York, 1989), Vol. 4, p. 119.

³R. N. Silver, Phys. Rev. B **37**, 3794 (1988).

⁴R. N. Silver, Phys. Rev. B **38**, 2283 (1988).

⁵R. N. Silver, in *Momentum Distributions*, edited by R. N. Silver (Plenum, New York, 1989).

⁶T. R. Sosnick, W. M. Snow, P. E. Sokol, and R. N. Silver, Europhys. Lett. **9**, 707 (1989).

⁷M. L. Ristig and J. W. Clark, Phys. Rev. B **40**, 4355 (1989).

⁸R. D. Amado, Phys. Rev. C **14**, 1264 (1976).

⁹R. D. Amado, Phys. Rev. C **16**, 1255 (1977).

¹⁰P. D. Zimmermann, C. F. Williamson, and Y. Kawazoe, Phys. Rev. C **19**, 279 (1979).

¹¹I. Sick, in *Progress in Particle and Nuclear Physics*, edited by A. Faessler (Pergamon, Oxford, 1985), Vol. 13.

¹²S. A. Gurvitz and A. S. Rinat, Phys. Rev. C **35**, 696 (1987);

Phys. Lett. **197B**, 6 (1987); A. S. Rinat, Phys. Rev. B **36**, 5171

(1987); **40**, 6625 (1989), and references cited therein.

¹³J. W. Clark and R. N. Silver, in *Proceedings of the Third International Conference on Nuclear Reaction Mechanisms*, Varenna, 1988, edited by E. Gadioli (Ricerca Scientifica ed Educazione Permanente, Università degli Studi di Milano, Milano, 1988), p. 531.

¹⁴M. L. Ristig and J. W. Clark, Phys. Rev. B **14**, 2875 (1976).

¹⁵S. Fantoni, Nuovo Cimento A **44**, 191 (1978).

¹⁶M. L. Ristig, in *From Nuclei to Particles*, Proceedings of the International School of Physics "Enrico Fermi," Course LVII, Varenna, 1981, edited by A. Molinari (North-Holland, Amsterdam, 1982), p. 340.

¹⁷D. Schiff and L. Verlet, Phys. Rev. **160**, 208 (1967).

¹⁸K. E. Kürten and J. W. Clark, Phys. Rev. B **30**, 1342 (1984).

¹⁹E. Feenberg, *Theory of Quantum Fluids* (Academic, New York, 1969).

²⁰J. W. Clark, in *Progress in Particle and Nuclear Physics*, edited by D. H. Wilkinson (Pergamon, Oxford, 1979), Vol. 2, p. 89.

²¹J. W. Clark and M. L. Ristig, in *Momentum Distributions*, edited by R. N. Silver (Plenum, New York, 1989).

²²J. W. Clark, Nucl. Phys. A **328**, 587 (1979).

- ²³J. E. Mayer and M. G. Mayer, *Statistical Mechanics* (Wiley, New York, 1940).
- ²⁴Q. N. Usmani, B. Friedman, and V. R. Pandharipande, *Phys. Rev. B* **25**, 4502 (1982).
- ²⁵Q. N. Usmani, S. Fantoni, and V. R. Pandharipande, *Phys. Rev. B* **26**, 6123 (1982).
- ²⁶M. Puoskari and A. Kallio, *Phys. Rev. B* **30**, 152 (1984); E. Manousakis, V. R. Pandharipande, and Q. N. Usmani, *Phys. Rev. B* **31**, 7022 (1985); M. F. Flynn, *ibid.* **33**, 91 (1986).
- ²⁷A. Fabrocini and S. Rosati, *Nuovo Cimento D* **1**, 567 (1982);
- D** **1**, 615 (1982); M. Viviani, E. Buendia, A. Fabrocini, and S. Rosati, *ibid.* **8**, 561 (1986).
- ²⁸M. Viviani, E. Buendia, S. Fantoni, and S. Rosati, *Phys. Rev. B* **38**, 4523 (1988).
- ²⁹E. Krotscheck, *Phys. Rev. A* **15**, 397 (1977).
- ³⁰F. Arias, E. Buendia, and M. Viviani (private communication).
- ³¹P. M. Lam, J. W. Clark, and M. L. Ristig, *Phys. Rev. B* **16**, 222 (1977).